



Title	Fast operation of a WO ₃ -based solid-state electrochromic transistor
Author(s)	Onozato, Takaki; Nezu, Yukio; Cho, Hai Jun; Ohta, Hiromichi
Citation	AIP Advances, 9(2), 025122 https://doi.org/10.1063/1.5089604
Issue Date	2019-02
Doc URL	http://hdl.handle.net/2115/75112
Rights	© 2019 Takaki Onozato, Yukio Nezu, Hai Jun Cho, and Hiromichi Ohta
Rights(URL)	https://creativecommons.org/licenses/by/4.0/
Type	article
File Information	1.5089604.pdf



[Instructions for use](#)

Fast operation of a WO_3 -based solid-state electrochromic transistor

Cite as: AIP Advances **9**, 025122 (2019); <https://doi.org/10.1063/1.5089604>

Submitted: 21 January 2019 . Accepted: 18 February 2019 . Published Online: 26 February 2019

Takaki Onozato, Yukio Nezu, Hai Jun Cho, and Hiromichi Ohta 



View Online



Export Citation



CrossMark

ARTICLES YOU MAY BE INTERESTED IN

Effects of vacuum annealing on the electron mobility of epitaxial La-doped BaSnO_3 films

APL Materials **7**, 022507 (2019); <https://doi.org/10.1063/1.5054154>

Large thickness dependence of the carrier mobility in a transparent oxide semiconductor, La-doped BaSnO_3

Applied Physics Letters **112**, 232102 (2018); <https://doi.org/10.1063/1.5033326>

Peculiar magnetotransport properties in $\text{La}_{0.67}\text{Sr}_{0.33}\text{MnO}_3/\text{LaAlO}_3/\text{SrTiO}_3$

AIP Advances **9**, 035129 (2019); <https://doi.org/10.1063/1.5079898>

AVS Quantum Science

Co-published with AIP Publishing



Coming Soon!

Fast operation of a WO₃-based solid-state electrochromic transistor

Cite as: AIP Advances 9, 025122 (2019); doi: 10.1063/1.5089604

Submitted: 21 January 2019 • Accepted: 18 February 2019 •

Published Online: 26 February 2019



Takaki Onozato,¹ Yukio Nezu,¹ Hai Jun Cho,^{1,2} and Hiromichi Ohta^{1,2,a)} 

AFFILIATIONS

¹Graduate School of Information Science and Technology, Hokkaido University, N14W9, Kita, Sapporo 060-0814, Japan

²Research Institute for Electronic Science, Hokkaido University, N20W10, Kita, Sapporo 001-0020, Japan

^{a)}Correspondence should be addressed to: H.O. (hiromichi.ohta@es.hokudai.ac.jp)

ABSTRACT

Electrochromic transistors (ECTs) have attracted attention as advanced memory technology because one can use both electrochromism and switching of electrical conductivity in a nonvolatile manner. Although several solid-state ECTs have been proposed so far, their operating speed is still slow (operating time >1 min) as compared to liquid-based ECTs (~20 s) due to their asymmetric gate-source electrode configuration. Here we demonstrate a fast operation of a solid-state ECT. We fabricated a solid-state ECT with three terminal gate-source-drain electrodes using an amorphous WO₃ film as the electrochromic material and amorphous TaO_x as the solid electrolyte. By the insertion of a thin ZnO layer between the source and drain electrodes to achieve pseudo symmetric gate-source electrode configuration, we greatly reduced the operation time to less than 1 s at ±3 V application while keeping the on-to-off ratio of ~30. The present approach is effective to improve the operating speed of ECTs and may be practically used in advanced memory technologies.

© 2019 Author(s). All article content, except where otherwise noted, is licensed under a Creative Commons Attribution (CC BY) license (<http://creativecommons.org/licenses/by/4.0/>). <https://doi.org/10.1063/1.5089604>

I. INTRODUCTION

Electrochromic transistors (ECTs), which are the combinations of electrochromic displays (ECDs) and three terminal transistors, have attracted attention as advanced memory devices because ECTs have advantages against conventional data storage devices, which can store 1 bit of information as 0 or 1.^{1,2} For example, WO₃-based ECT channel turns from high resistive to low resistive state when the positive gate voltage is applied. At the same time, the color of the ECT channel turns from almost colorless transparent into dark blue. Thus, ECT can store the information of electrical resistance and color simultaneously in a nonvolatile manner.^{2,3}

Although many EC materials including organic materials are reported thus far,^{4–6} WO₃ has been considered as one of the best EC materials to develop ECT because WO₃ has several advantages such as large on/off ratio of the electrical conductivity and the large color contrast ratio. Several researchers have investigated the structural phase transition and metal-insulator transition using a liquid electrolyte and an epitaxial WO₃ film thus far.^{7–10} In 2015, Barquinha *et al.* demonstrated amorphous WO₃-based ECT prepared on a paper substrate.² Very recently, neuromorphic transistor,^{11,12}

which imitated synaptic movements, has been developed using WO₃-ECTs. Previously, most researchers used liquid electrolytes to fabricate WO₃-based ECT, however, the use of a liquid is not suitable for the practical application due to the leakage problem. To overcome this problem, several researchers used solid electrolytes to fabricate WO₃-based ECTs,^{3,13} which are free from the leakage issues. However, the operating speed of solid-state WO₃-based ECTs is slow (operating time >1 min^{3,13}) as compared to liquid-based ECTs (~20 s²), most likely due to that the ionic conductivity of liquid electrolytes is higher than that of solid electrolyte.

In order to overcome this issue, we compared to the device structure of WO₃-based ECTs and WO₃-based electrochromic displays (ECDs) because ECDs can be operated within several milliseconds.^{6,14} Figure 1 schematically illustrates the structural difference between an ECD and an ECT. Both devices are composed of WO₃, electrolyte, and NiO, which are sandwiched by two transparent conducting oxides (TCOs). Protonation of WO₃ occurs when the electric field is applied to the multilayered structure composed of the top TCO electrode, NiO, electrolyte, WO₃ and the bottom electrode. Therefore, the multilayers are sandwiched by the two ITO electrodes with fully overlapped parallel plate electrode configuration in the

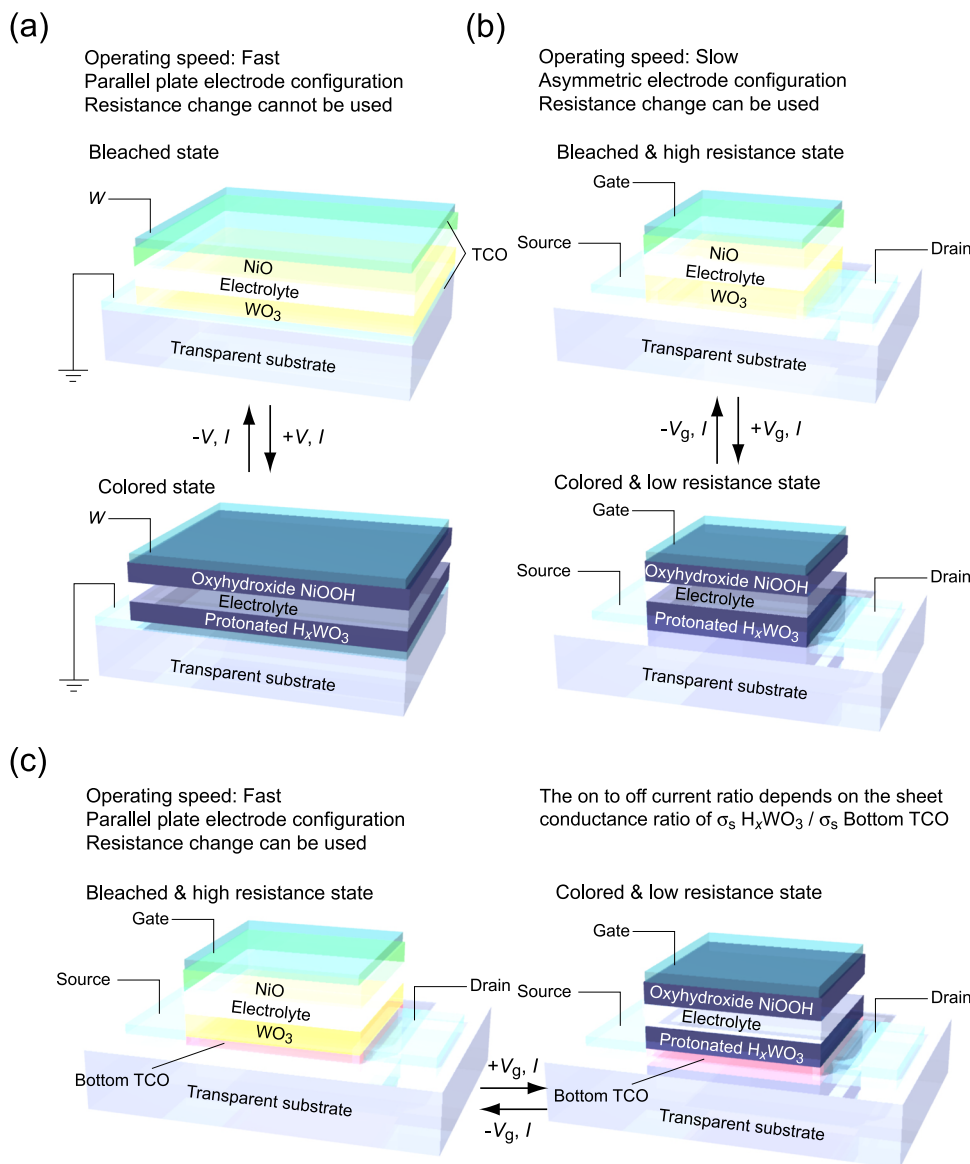


FIG. 1. Electrochromic devices. Schematic device structures of (a) electrochromic displays (ECDs), (b) reported electrochromic transistor, and (c) present electrochromic transistor. All devices are composed of WO₃, electrolyte, and NiO, which are sandwiched by two ITO (a transparent conducting oxide, ITO). Since there is a parallel plate electrode configuration, the operating speed of (a) is much faster than that of (b), of which the electrode configuration is asymmetric. Although one can use the resistance change in the case of (b), it cannot be used in the case of (a). In order to overcome this dilemma, we would like to propose the device structure (c), which is three terminal thin film transistor structure with parallel plate electrode configuration. We expected that the device (c) exhibits both fast transistor-like characteristic as well as the electrochromic display characteristics.

case of conventional ECD as shown in Fig. 1(a). On the contrary, in the case of reported three terminal ECT, the overlap area of the gate and source is very small as compared to the whole area of the multilayer as shown in Fig. 1(b). Hence the protonation occurs at the WO₃ layer near the source electrode firstly, and then it gradually proceeds to the drain electrode side. Since both ECTs and ECDs utilize the electrochemical reaction of WO₃ and proton [$\text{WO}_3 + x\text{H}^+ + xe^- \leftrightarrow \text{H}_x\text{WO}_3$], the flowing current in the whole WO₃ film dominates the operation speed. Thus, the operation speed of the reported ECTs with asymmetric electrode configuration is slower than that of ECDs and liquid-based ECTs.

Here we show a fast operation of a solid-state WO₃-based ECT. We fabricated a three terminal thin film solid-state ECT with a pseudo parallel plate electrode configuration as shown in Fig. 1(c).

We inserted thin oxygen deficient ZnO^{15,16} layer, which is known as an n-type wide bandgap ($E_g = 3.4$ eV) semiconductor, as the bottom TCO between the source and drain electrodes to achieve pseudo symmetric gate-source electrode configuration. As a result, we greatly reduced the operation time to less than 1 s at ± 3 V application while keeping the on-to-off ratio of ~ 30 . The present approach is effective to improve the operating speed of ECTs and may be practically used in advanced memory technologies.

II. EXPERIMENTAL

The ECT devices were fabricated on an alkaline-free glass substrate (Corning EAGLE XG, $10 \times 10 \times 0.7$ mm) by pulsed laser deposition (PLD) with KrF excimer laser (248 nm, 10 Hz)

using stencil masks as shown in Figs. 2(a) and 2(b). All film fabrication processes were conducted at room temperature. (see experimental section for the detail). At first, a 30-nm-thick oxygen deficient ZnO film with the sheet conductance of $\sim 150 \mu\text{S}$, which is more than two orders of magnitude smaller than that of

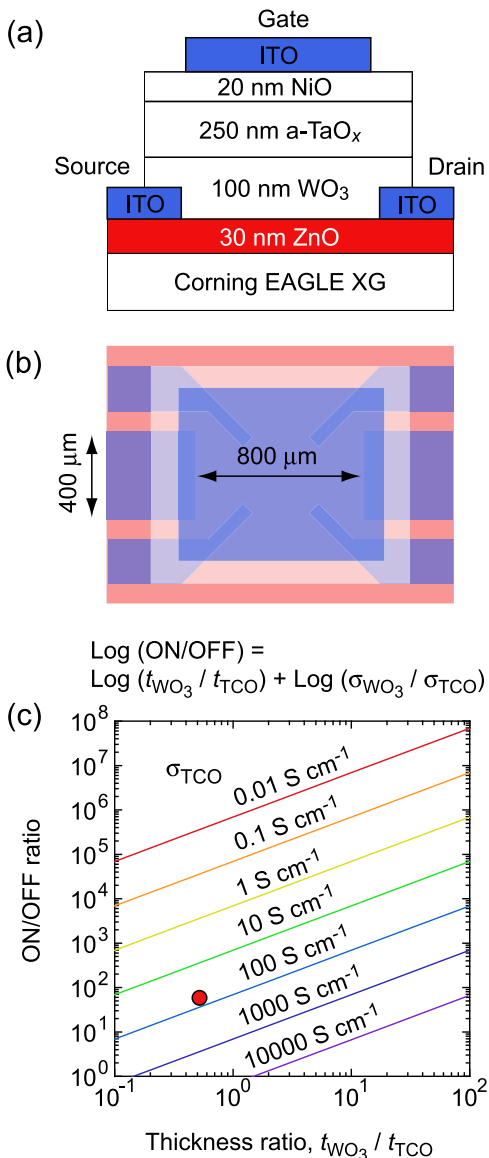


FIG. 2. Present electrochromic transistor with the bottom TCO layer. (a) Schematic cross-sectional and (b) top view of the electrochromic transistor device. We fabricated the device on Corning EAGLE XG glass substrate. Using the stencil masks, we deposited ZnO as the bottom TCO layer (30 nm), ITO as the source and the drain electrodes, a-WO₃ layer (100 nm), solid-electrolyte a-TaO_x (250 nm) layer, and NiO layer. The active channel size is 800 μm in length and 400 μm in width. (c) We roughly hypothesized that the on-to-off current ratio depends on the thickness ratio of WO₃ and the TCO if we fix the electrical conductivity of the TCO (σ) (We assumed that the σ of HWO₃ is 7000 S cm^{-1}). The red circle is showing the point of the present result.

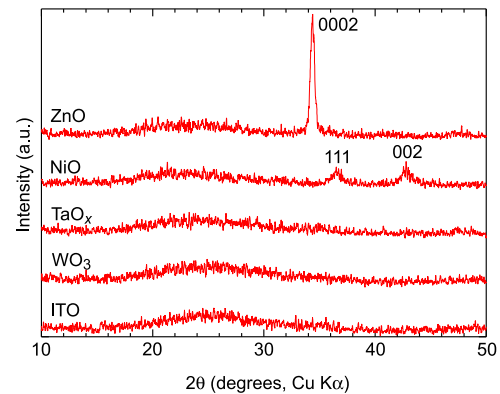


FIG. 3. Glancing incidence XRD patterns of each layer of the present device. In the case of ZnO and NiO films, diffraction peaks of 0002 ZnO, and 111 and 002 NiO are seen, whereas only halo patterns are seen in TaO_x, WO₃, and ITO. These results clearly indicate that the TaO_x, WO₃, and ITO layers are amorphous, whereas ZnO and NiO are randomly oriented polycrystalline.

protonated WO₃ ($\sim 70 \text{ mS}$), was deposited on the substrate as the bottom TCO layer. The electrical conductivity, carrier concentration, and Hall mobility of the ZnO layer were $\sim 50 \text{ S cm}^{-1}$, $\sim 5 \times 10^{-19} \text{ cm}^{-3}$, and $\sim 6.6 \text{ cm}^2 \text{ V}^{-1} \text{ s}^{-1}$, respectively, at room temperature. Then the source and drain electrodes (a-ITO), a-WO₃ active layer (100 nm), a-TaO_x electrolyte (250 nm), NiO counter layer (20 nm), and gate electrode (a-ITO) were deposited sequentially using the stencil masks [Fig. 2(a)]. The active channel size was 800 μm in length and 400 μm in width as schematically shown in Fig. 2(b). The ITO, WO₃ and TaO_x films were amorphous, whereas the ZnO and NiO films were polycrystalline [Fig. 3], which was analyzed by glancing incidence (ω -fixed 2θ scan) X-ray diffraction (Cu K α_1 , ATX-G, Rigaku Co.).

Since we inserted a thin ZnO layer as a thin TCO, the electrical resistance switching ON/OFF ratio should be lower than reported without bottom TCO layer ECT device (ON/OFF ratio $\sim 10^6$). The ON/OFF ratio can be controlled using the following equation, which describes the relationship between t_{WO_3} and t_{TCO} : $\log(\text{ON/OFF}) = \log(t_{\text{WO}_3}/t_{\text{TCO}}) + \log(\sigma_{\text{WO}_3}/\sigma_{\text{TCO}})$. Figure 2(c) shows the calculated ON/OFF ratio as a function of the thickness ratio of $t_{\text{WO}_3}/t_{\text{TCO}}$. Since we used a 30-nm-thick ZnO ($\sim 50 \text{ S cm}^{-1}$), the maximum ON/OFF ratio was calculated to be ~ 50 (filled red circle). It should be noted that there is a trade-off relationship between the ON/OFF ratio and the operating time. In order to increase the operating speed while keeping moderate ON/OFF ratio, we used a 30-nm-thick ZnO film.

III. RESULTS AND DISCUSSION

The present ECT with the TCO layer could be operated very fast. Figure 4(a) shows the changes in the sheet resistance (R_s) of the present ECT (w/TCO) as a function of time for both the protonation (gate voltage, $V_g = +3 \text{ V}$, left) and deprotonation ($V_g = -3 \text{ V}$, right) stages at room temperature. The gate current (I_g) during V_g application was measured by using a source measure unit (Keithley 2450). R_s was measured by the d.c. four probe method in the van der

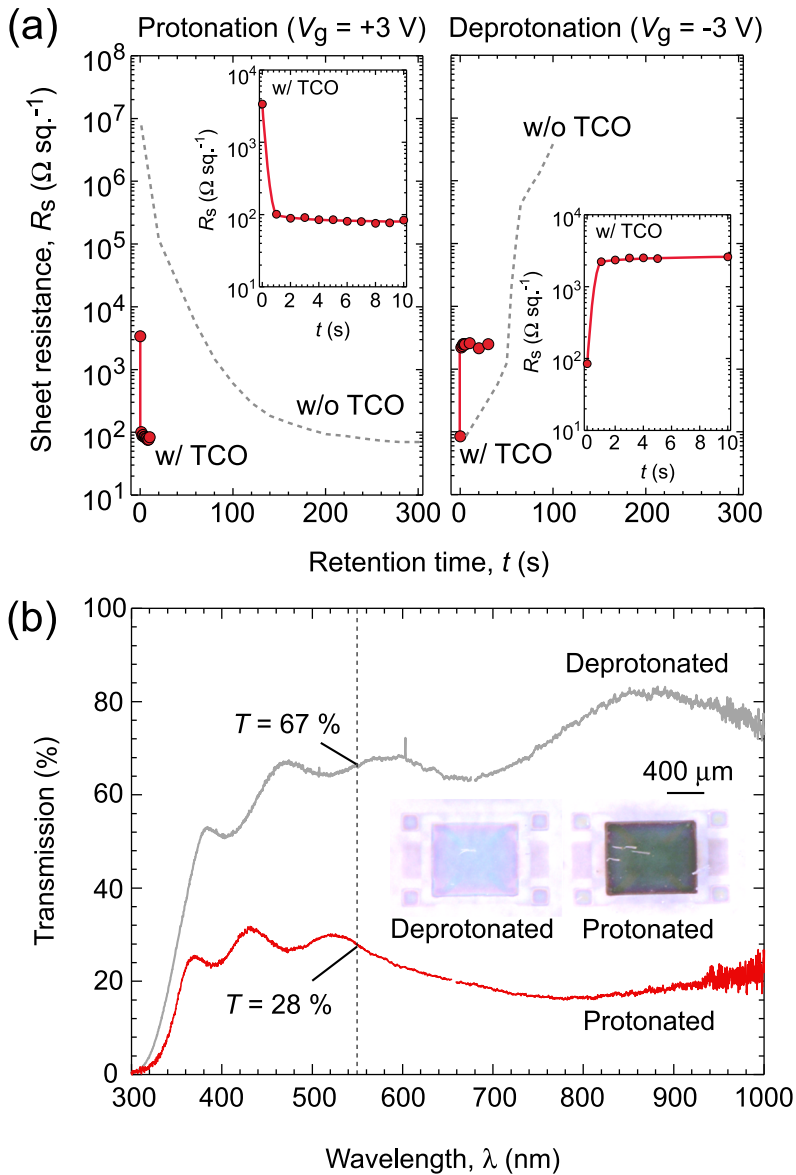


FIG. 4. Change in the sheet resistance and the optical transmission before and after the protonation. (a) The decay of the sheet resistance (R_s) when +3 V is applied (left) and recovering of R_s when -3 V is applied. The result without the bottom TCO is also shown for comparison (dotted lines). The R_s drops within 1 s when +3 V is applied, whereas the R_s increases within 1 s when -3 V is applied. The operation time of the present device is much faster than the device without the TCO layer. (b) Optical transmission spectra of the present device. The transmission (T) of the deprotonated state (gray line) is 67 % at 550 nm whereas as the protonated state shows 28 % at $\lambda = 550$ nm. The inset shows the photographs of the device. After the protonation, the device becomes dark blue whereas the device was transparent at the deprotonated state.

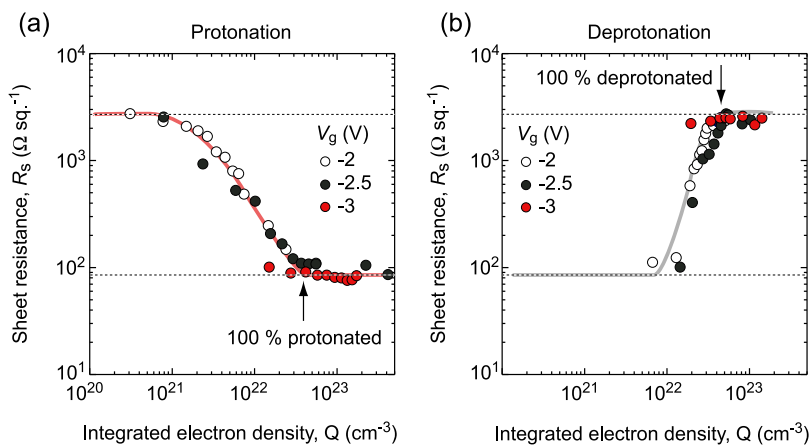


FIG. 5. Sheet resistance of the device as a function of the integrated electron density (Q). Details of the calculation process of charge electron-density are described elsewhere.^{3,17} To achieve 100 % protonation/oxidation, $Q = 1.5 \times 10^{22} \text{ cm}^{-3}$ is required based on our electrochromic reaction: $\text{WO}_3 + x\text{H}^+ + x\text{e}^- \rightarrow \text{H}_x\text{WO}_3$. The present ECT device obeys the Faraday's laws of electrolysis. (a) The R_s gradually decreases from $3 \times 10^3 \Omega \text{ sq}^{-1}$ to $8 \times 10^1 \Omega \text{ sq}^{-1}$ with increasing Q and saturates when Q is $4 \times 10^{22} \text{ cm}^{-3}$. (b) The R_s increases from $8 \times 10^1 \Omega \text{ sq}^{-1}$ to $3 \times 10^3 \Omega \text{ sq}^{-1}$ with increasing Q and saturates when Q is $4 \times 10^{22} \text{ cm}^{-3}$.

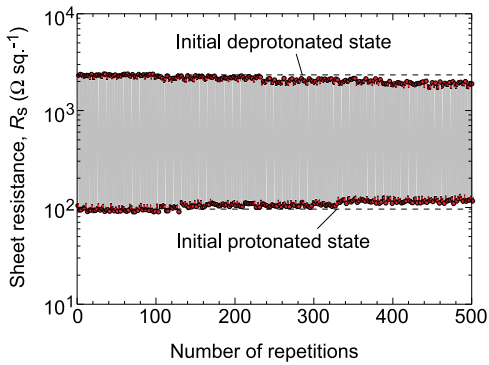


FIG. 6. Cycle characteristics of the electrochromic transistor device. Repetitive property of the electrochromic device by applying repeatedly at $V_g = \pm 3$ V for 2 s. After 500 repetitions, the cyclability is more than 90 %.

Pauw electrode configuration. The R_s of the ECT without the TCO layer is also shown for comparison (dotted line). When we applied $V_g = +3$ V, the R_s of the present ECT dropped from $\sim 3000 \Omega \text{ sq}^{-1}$ to $\sim 100 \Omega \text{ sq}^{-1}$ within 1 s. The ON/OFF ratio was ~ 30 , which is similar to the maximum ON/OFF ratio described above. On the other hand, the ECT w/o TCO showed very slow decay of R_s ; the R_s changed slowly taking > 50 s from $\sim 10^7 \Omega \text{ sq}^{-1}$ to $\sim 90 \Omega \text{ sq}^{-1}$. Thus, the operating speed was $\sim 20 \mu\text{m s}^{-1}$, which correspond to the time to protonate from the edge of source electrode to the edge of the drain electrode. In case of deprotonation, the present ECT showed fast recovery of R_s within 1 s. It should be noted that the operation of the present ECT device obeys Faraday's laws of electrolysis (Fig. 5).^{3,17} These results clearly indicate that the present ECT with TCO layer can operated at a much faster speed as compared to the ECT without the TCO layer.

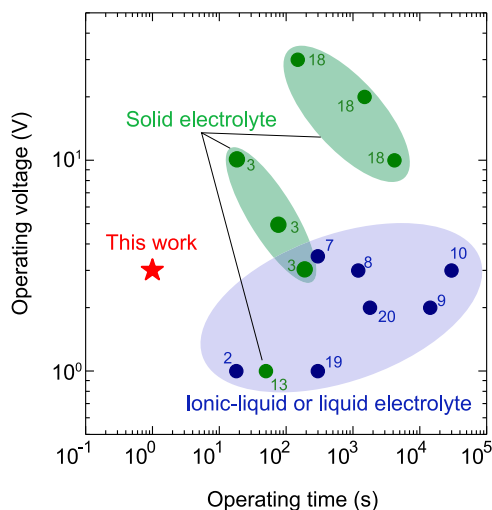


FIG. 7. The operating voltage vs. the operating time. The operating time and voltage of the present device is 3 V and less than 1 s (red star), which are smaller than that of the reported solid electrolyte devices (green)^{5,13,18} and ionic liquid or liquid electrolyte devices (blue).^{2,7-10,19,20}

Then, we measured the optical transmission change of the present ECT [Fig. 4(b)]. The transmission (T) of the deprotonation state was 67 % at the wavelength (λ) of 550 nm and has a high overall transmittance in the visible region. After a gate voltage application of +3 V, the transmittance dramatically decreased to 28 % at $\lambda = 550$ nm, and the average transmittance in the visible region was greatly reduced (see the video of the optical transmission spectrum during the device operation at [supplementary material](#)). To check the cyclability of the present ECT, we applied alternating $V_g = \pm 3$ V at 4 s period (i.e. 2 s at +3 V and 2 s at -3 V) and monitored the sheet resistance (Fig. 6). Cyclability over 90 % was achieved after 500 repetitions, which ensures the good reversibility of the present ECT device.

Figure 7 shows a comparison between the present WO_3 -based ECT and the reported WO_3 -based ECTs (solid-state ECTs^{3,13,18} and liquid electrolyte ECTs^{2,7-10,19,20}). The operating voltage and the operating time of the present ECT were ± 3 V and ~ 1 s, respectively. Since there is an inverse proportional relationship between the operating voltage and the operating time, our result shows that the insertion of a thin TCO in solid-state WO_3 -based ECTs is effective to greatly reducing both operating voltage and speed. Although current operating time (~ 1 s) is difficult to use as the memory cell of the flash memory ($\sim \mu\text{s}$), the operating time would be enough fast for smart display applications. Thus, the present approach may be practically used in advanced memory technologies.

IV. CONCLUSIONS

In conclusions, we have demonstrated that a solid state WO_3 -based ECT with TCO bottom layer can be operated faster (~ 1 s) than the reported WO_3 -based ECTs (solid-state: ~ 1 min, liquid electrolytes: ~ 20 s) at low operation voltage (± 3 V) keeping the ON/OFF ratio ~ 30 . Since all fabrication processes were performed at room temperature, the present ECT can be fabricated not only on glass substrates but also on flexible substrates such as plastics, which will have significant economic advantages. We envision that this new EC device structure will move the EC technology forward and be utilized in advanced memory devices.

SUPPLEMENTARY MATERIAL

See [supplementary material](#) for the movie showing fast operation of the electrochromic transistor.

ACKNOWLEDGMENTS

This research was supported by Grants-in-Aid for Scientific Research A (17H01314), the Asahi Glass Foundation, and the Mitsubishi Foundation. Student aids from JSPS (T.O., 17J01281) is also greatly appreciated.

REFERENCES

- H. Akinaga and H. Shima, *Proc. IEEE* **98**, 2237–2251 (2010).
- P. Barquinha, S. Pereira, L. Pereira, P. Wojcik, P. Grey, R. Martins, and E. Fortunato, *Adv. Electron. Mater.* **1**, 1500030 (2015).
- T. Katase, T. Onozato, M. Hirono, T. Mizuno, and H. Ohta, *Sci. Rep.* **6**, 25819 (2016).
- D. Y. Tu, D. Nilsson, and R. Forchheimer, *J Disp Technol* **9**, 755–759 (2013).

- ⁵Z. Li, Y. Zhang, A. L. Holt, B. P. Kolasa, J. G. Wehner, A. Hampf, G. C. Bazan, T.-Q. Nguyen, and D. E. Morse, *New J. Chem.* **35**, 1327 (2011).
- ⁶V. Jain, H. M. Yochum, R. Montazami, and J. R. Heflin, *Appl. Phys. Lett.* **92**, 033304 (2008).
- ⁷M. Wang, S. Shen, J. Ni, N. Lu, Z. Li, H. B. Li, S. Yang, T. Chen, J. Guo, Y. Wang, H. Xiang, and P. Yu, *Adv. Mater.* **29**, 1703628 (2017).
- ⁸S. G. Altendorf, J. Jeong, D. Passarello, N. B. Aetukuri, M. G. Samant, and S. S. Parkin, *Adv. Mater.* **28**, 5284–5292 (2016).
- ⁹X. Leng, J. Pereiro, J. Strle, G. Dubuis, A. T. Bollinger, A. Gozar, J. Wu, N. Litombe, C. Panagopoulos, D. Pavuna, and I. Bozovic, *Npj Quantum Mater* **2**, 35 (2017).
- ¹⁰C. ViolBarbosa, J. Karel, J. Kiss, O. D. Gordan, S. G. Altendorf, Y. Utsumi, M. G. Samant, Y. H. Wu, K. D. Tsuei, C. Felser, and S. S. Parkin, *Proc. Natl. Acad. Sci. USA* **113**, 11148–11151 (2016).
- ¹¹J. T. Yang, C. Ge, J. Y. Du, H. Y. Huang, M. He, C. Wang, H. B. Lu, G. Z. Yang, and K. J. Jin, *Adv. Mater.* **30**, 1801548 (2018).
- ¹²T. Tsuchiya, M. Jayabalan, K. Kawamura, M. Takayanagi, T. Higuchi, R. Jayavel, and K. Terabe, *Jpn. J. Appl. Phys.* **57**, 04fk01 (2018).
- ¹³P. Grey, L. Pereira, S. Pereira, P. Barquinha, I. Cunha, R. Martins, and E. Fortunato, *Adv. Electron. Mater.* **2**, 1500414 (2016).
- ¹⁴T. Niwa and O. Takai, *Thin Solid Films* **518**, 1722–1727 (2010).
- ¹⁵T. Minami, H. Nanto, and S. Takata, *Appl. Phys. Lett.* **41**, 958–960 (1982).
- ¹⁶R. E. I. Schropp and A. Madan, *J. Appl. Phys.* **66**, 2027–2031 (1989).
- ¹⁷T. Katase, Y. Suzuki, and H. Ohta, *Adv. Electron. Mater.* **2**, 1600044 (2016).
- ¹⁸S. Thakoor, A. Moopenn, T. Daud, and A. P. Thakoor, *J. Appl. Phys.* **67**, 3132–3135 (1990).
- ¹⁹X. Meng, F. Quenneville, F. Venne, E. Di Mauro, D. Işık, M. Barbosa, Y. Drollet, M. M. Natile, D. Rochefort, F. Soavi, and C. Santato, *J. Phys. Chem. C* **119**, 21732–21738 (2015).
- ²⁰H. Kalthori, M. Coey, I. Abdolhosseini Sarsari, K. Borisov, S. B. Porter, G. Atchison, M. Ranjbar, H. Salamati, and P. Stamenov, *Sci Rep* **7**, 12253 (2017).